International Journal for Numerical Methods in Engineering

A Computational Framework for Dynamic Data Driven Material Damage Control, Based on Bayesian Inference and Model Selection

E. E. Prudencio, P. T. Bauman, D. Faghihi,
K. Ravi-Chandar, and J. T. Oden*

Institute for Computational Engineering and Sciences (ICES)
The University of Texas at Austin
201 East 24th St, Stop C0200, Austin, Texas 78712-1229, USA

It is with great pleasure that we contribute this study in honor of our dear colleague, friend, and visionary in the field of numerical methods in engineering, Professor Ted Belytschko. We thank him for his numerous contributions to this field, for his statesmanship, and for his leadership over the many years of development of the subject of computational engineering.

Abstract

In the present study a general Dynamic Data-Driven Application System (DDDAS) is developed for real-time monitoring of damage in composite materials using methods and models that account for uncertainty in experimental data, model parameters, and in the selection of the model itself. The methodology involves (1) data of the uni-axial tensile experiments conducted on a composite material; (2) continuum damage mechanics based material constitutive models; (3) Bayesian framework for uncertainty quantification, calibration, validation, and selection of models; and (4) general Bayesian filtering, as well as Kalman and extended Kalman filters. A software infrastructure is developed and implemented in order to integrate the various parts of the DDDAS. The outcomes of computational analyses using the experimental data prove the feasibility of the Bayesian-based methods for model calibration, validation, and selection. Moreover, using such DDDAS infrastructure for real-time monitoring of the damage and degradation in materials results in an advance prediction of failure in the system.

Key Words: *Bayesian model selection, extended Kalman filter, Dynamic Data Driven Application Systems, material damage.*

1 Introduction

With repeated loading cycles or accidental overloading such as foreign-object impact events, composite materials accumulate damage that degrades their performance and eventually leads to failure. Therefore, it is very important to monitor and track the evolution of damage in these composite materials. The ability to obtain continuous updates in the health of the

*Corresponding author, oden@ices.utexas.edu

structure provides a large collection of data that can be coupled within the framework of a Dynamically Data Driven Application System (DDDAS) in order to extract appropriate conclusions regarding structural durability and reliability. The types and evolution of damage that appear in composite materials and structures are complex functions of the composition, architecture, geometry and loading history.

The underlying philosophy of DDDAS is to connect the dynamic computational models of the evolution of physical phenomena of interest with the experimental systems that deliver relevant data in near-real time so as to allow feedback to control outputs to meet a set of objectives (see [10, 11, 12, 13, 14, 15, 16]).

The present study develops a stochastic DDDAS for prediction and monitoring of material damage in composite materials common to many types of contemporary high-performance military aircraft. In this regard, the computational models are based on finite element approximation of highly nonlinear material damage theories of the type used in contemporary fatigue analysis, fracture mechanics, and structural mechanics. These typically involve material parameters that exhibit uncertainties. In order to provide information for real-time monitoring of damage, the dynamically collected data of uniaxial tensile experimental conducted on composite materials [4] is taken into consideration. Thus, the system itself must be calibrated and validated, and the inherent uncertainties in data must be factored into a statistical analysis for the validation of the full system. A Bayesian framework is also developed for defining, updating, and quantifying uncertainties in the model, the experimental data, and the target quantities of interest.

This paper is structured as follows. A summary of some physical models for damage that are considered for adoption along with the finite element solution procedure is presented in Section 2. This is followed by Section 3, by the development of a corresponding DDDAS. In Section 4, the experimental results used in the statistical analyses are presented. Bayesian methods for model calibration, validation, and selection with quantification of uncertainties are outlined in Section 5. Section 6 describes the developed and implemented software infrastructure in order to integrate the acquired experimental data along with the finite element solution of the continuum damage mechanics model in order to calibrate the model and compute model plausibilities that guide the selection of the models themselves. This is accomplished with real-time monitoring of damage using the Bayesian filtering algorithms. The results of statistical calibration of damage models, damage models ranking, and damage monitoring, given the experimental measurements of the composite material, are presented in Section 7. Summary and conclusions are collected in Section 8.

2 Continuum Damage Mechanics

A material under loading is regarded as damaged relative to some initial state when it experiences a loss of stiffness due to the emergence of microscale defects (e.g. micro-cracks, micro-voids). In contrast to fracture mechanics, continuum damage mechanics is based on the idea of the existence of a damage field, which measures the density of these micro-defects. An increase in damage signals a deterioration of the material before the initiation of macro-cracks. The notion of a damage density field was first introduced by Kachanov [21], who postulated an evolution equation for the growth of damage, written in terms

of stress or strain, which may be used to predict the failure of material. More general models of anisotropic damage were introduced by Chaboche [6, 7], Murakami and Ohno [27], Krajcinovic and Foneska [23] and others, in which the damage variable can be tensorial to account for anisotropy in the material properties in failure mode. Here we restrict ourselves to isotropic damage, which consists of cracks and cavities with an orientation distributed uniformly in all directions. The assumption of isotropic damage with scalar damage field is often regarded as sufficient to give a good prediction of the load carrying capacity, the number of cycles or the time to local failure in isotropic structural components. In this case, the damage variable does not depend on the orientation and the damaged state and is completely characterized by a scalar field $D = D(\mathbf{x}, t)$. It is common to scale the damage measure so that the value $D = 0$ characterizes the virgin (undamaged) state, while $D = D_c \leqslant 1$ characterizes the initiation of a macro-crack. The parameter D_c is a critical value for the damage variable usually taken between 0.2 and 0.8 for engineering materials (see the references in Lemaître and Chaboche [25]). It is commonly agreed in continuum damage mechanics that, once a material is damaged, further loading only affects the undamaged (intact) material skeleton. This motivates the development of several classes of constitutive equations (model classes) for the evolution of the damage field, all designed to predict the progression of micro-cracks in the course of elastic and plastic deformation of various materials.

Generally, the damage evolution, $\dot{D}$, can be a function of the stress tensor $\boldsymbol{\sigma}$, hydrostatic stress $\mathrm{tr}\boldsymbol{\sigma}$, strain tensor $\boldsymbol{\epsilon}$, strain rate $\dot{\boldsymbol{\epsilon}}$, temperature T, and damage history D such that the evolution of damage is assumed to be governed by an constitutive equation of the type

$$\dot{D} = \mathcal{F}(\boldsymbol{\sigma}, \mathrm{tr}\boldsymbol{\sigma}, \boldsymbol{\epsilon}, \dot{\boldsymbol{\epsilon}}, D, T). \tag{1}$$

Kachanov [21] was the first to postulate an evolution equation of creep damage based on a power law of the form

$$\dot{D} = \left[\frac{\sigma}{c_1(1-D)}\right]^{c_2}, \tag{2}$$

where c_1 and c_2 are material constants depending upon the temperature, and σ is the applied (uniaxial) stress. Belloni et al. [5] proposed the creep damage law

$$\dot{D} = (\delta+1)c\epsilon^{\alpha}\left[\exp\left(-\frac{\beta}{T}\right)\right]\sigma^{\gamma}t^{\delta}, \tag{3}$$

where $c, \alpha, \beta, \gamma, \delta$ are material constants, and t is time. Later, relying on several sets of experiments, it was argued that strain is the most important variable in the evolution of damage variable (e.g. Cozzarelli and Bernasconi [9] and Lee at al. [24]). Considering the effect of damage on the elastic stiffness, Krajcinovic and Foneska [23] postulated the following power law for the damage evolution in brittle materials

$$\dot{D} = (s+1)\frac{\epsilon^{s}}{\epsilon_{\mathrm{R}}^{(s+1)}}\dot{\epsilon}, \tag{4}$$

where s is a material constant and ϵ_{R} can be interpreted as the final strain at rupture. Extending the Krajcinovic damage model, Marigo [26] considered volume effects, for which

the probability of microscale defects increases with increasing volume. An evolution equation for this type of damage thus the form

$$\dot{D} = \frac{2E^{2\alpha}\epsilon(D-1)}{\beta^{\alpha}}\dot{\epsilon}, \tag{5}$$

where E is Young's modulus, α is called the Weibull modulus, and β is the ultimate stress to rupture of a hypothetical sample without any defect.

Each aforementioned model class, M_j, contains materials parameters, represented in parameter vector $\boldsymbol{\theta_j}$, in order to capture the damage and degradation responses. In calibrating such material parameters against experimental data, uncertainties must be taken into account. Regardless of the physical justification behind each model, the question is, in a set of model classes, $\mathcal{M} = \{M_1, M_2, ...\}$, which class is the most plausible to address the damage behavior in a particular material for given experimental data. In this work, an answer to this question is proposed based on a Bayesian analysis of damage models and of experimental data collected from composite material body that accounts for the damage evolution.

2.1 Mathematical Models of Material Damage

Consider a material body occupying an open bounded domain $\Omega \subset \mathbb{R}^3$ with smooth boundary $\partial\Omega$. Local linear and angular momentum balances are governed by the equations

$$\boldsymbol{\nabla}.\boldsymbol{\sigma}(\mathbf{x}, t) + \mathbf{f}(\mathbf{x}) = 0, \qquad \forall\ \mathbf{x} \in \Omega \text{ and } t > 0, \tag{6}$$

and

$$\boldsymbol{\sigma}(\mathbf{x}, t) = \boldsymbol{\sigma}(\mathbf{x}, t)^T, \qquad \forall\ \mathbf{x} \in \Omega \text{ and } t > 0, \tag{7}$$

where $\boldsymbol{\sigma}(\mathbf{x}, t)$ is the Cauchy stress at point $\mathbf{x}$ on Ω at time t and $\mathbf{f}(\mathbf{x})$ is body force acting within Ω. On the boundary we have

$$\mathbf{g}(\mathbf{x}, t) = \boldsymbol{\sigma}(\mathbf{x}, t)\mathbf{n}, \qquad \forall\ \mathbf{x} \in \Gamma_\sigma. \tag{8}$$

where $\mathbf{g}(\mathbf{x}, t)$ are prescribed tractions on surface $\Gamma_\sigma \subset \partial\Omega$ and $\mathbf{n}$ denotes the outward unit normal to $\partial\Omega$.

The loss of elastic stiffness due to material damage is expressed the form of the reduced stress tensor,

$$\boldsymbol{\sigma} = (1 - D)\ \mathbb{C}\ \boldsymbol{\epsilon}, \tag{9}$$

where $\mathbb{C}$ is the fourth-order elastic tensor, and $\boldsymbol{\epsilon}$ is the strain tensor,

$$\boldsymbol{\epsilon} = \frac{1}{2}\left(\boldsymbol{\nabla}\mathbf{u} + (\boldsymbol{\nabla}\mathbf{u})^T\right). \tag{10}$$

with $\boldsymbol{\nabla}\mathbf{u}$ the displacement gradient.

Moreover, by postulating a proper form of energy dissipation due to material damage, one can write the following damage criterion (see [4]),

$$Y \leq \omega(\boldsymbol{\theta}, D), \tag{11}$$

where Y is the effective elastic energy density

$$Y = \boldsymbol{\epsilon} : \mathbb{C}\boldsymbol{\epsilon}, \tag{12}$$

and $\omega(\boldsymbol{\theta}, D)$ is the threshold of damage, for the particular damage model in use.

As mentioned in the beginning of this section, several evolution equations exist for damage variable that provide different functions ω for predicting the material failure. For example, two simple damage models, proposed by Krajcinovic and Foneska [23] and Marigo [26] are listed as follows.

- Krajcinovic Damage Model:

$$\omega = \frac{1}{2} E \epsilon_R^2 D^{\left(\frac{2}{s+1}\right)}, \tag{13}$$

- Marigo Damage Model:

$$\omega = \frac{1}{2} \frac{\beta^{2\alpha}}{E^{2\alpha - 1}} \ln\left(\frac{1}{1-D}\right), \tag{14}$$

2.2 Finite Element Approximation

Introducing the constitutive relationships into the momentum equation (6), in the absence of body forces,

$$\left.\begin{array}{rcll} \boldsymbol{\nabla}.\boldsymbol{\sigma}^{(k+1)} & = & 0 & \forall\ \mathbf{x} \in \Omega, \\ \mathbf{u}^{(k+1)} & = & \mathbf{u}_0(\mathbf{x}, t^{(k+1)}) & \forall\ \mathbf{x} \in \Gamma_u, \\ \boldsymbol{\sigma}^{(k+1)}\mathbf{n} & = & \mathbf{g}_0(\mathbf{x}, t^{(k+1)}) & \forall\ \mathbf{x} \in \Gamma_\sigma, \end{array}\right\}, \tag{15}$$

for each time increment $t^{(k+1)}$ where $\mathbf{u}_0$ and $\mathbf{g}_0$ are the prescribed displacement and traction respectively.

A weak form of these equations is obtained by introducing (9), multiplying them by an admissible test function $\boldsymbol{v}$, and integrating by parts. We now consider the evolution of damage governed by (1) over time interval $(0, T]$, which is partitioned into sub-intervals $[t^{(k)}, t^{(k+1)}]$, $k = 1 \ldots N_t$. Denoting the stress and displacement at point $\mathbf{x} \in \Omega$ and at time $t^{(k+1)}$ by $\boldsymbol{\sigma}^{(k+1)}(= \boldsymbol{\sigma}(\mathbf{x}, t^{(k+1)}))$ and $\mathbf{u}^{(k+1)}(= \mathbf{u}(\mathbf{x}, t^{(k+1)}))$, we arrive at the incremental equation,

$$\int_\Omega (1 - D^{(k+1)})\ \mathbb{C}\ \nabla \mathbf{u}^{(k+1)}\ .\ \nabla \boldsymbol{v}\ \mathrm{d}x = \int_{\Gamma_\sigma} \mathbf{g}_0(\mathbf{x}, t^{(k+1)})\ .\ \boldsymbol{v}\ \mathrm{d}s, \qquad \forall\ \boldsymbol{v} \in \mathcal{V} \tag{16}$$

for an appropriate space of test functions,

$$\mathcal{V} = \{\boldsymbol{v}(\mathbf{x}) \mid \boldsymbol{v}(\mathbf{x}) \in H^1(\Omega)\ ;\ \boldsymbol{v}(\mathbf{x}) = 0,\ \forall\ \mathbf{x} \in \Gamma_u\}, \tag{17}$$

where H^1 is the Sobolev space of functions with first-order generalized derivatives in $L^2(\Omega)$. Finite element approximations of the problem are obtained by considering the sub-spaces $\mathcal{V}^h \subset \mathcal{V}$.

Here, the damage field is also discretized using a possibly different basis from that of the finite element approximation for displacement $\mathbf{u}^h$. Thus, one can rewrite the weak form (16) as a system of nonlinear equations

$$\int_\Omega \boldsymbol{\sigma}\left(\mathbf{u}^h(t^{(k+1)}), D^h(t^{(k+1)})\right) \nabla \mathbf{N}\ \mathrm{d}x - \int_{\Gamma_\sigma} \mathbf{g}_0(t^{(k+1)})\ .\ \mathbf{N}\ \mathrm{d}s = 0. \tag{18}$$

where $\mathbf{N}(\mathbf{x})$ is the vector of nodal shape function.

Since stress depends upon the the history of $\mathbf{u}$ and D, the key is the evaluation of the stress state $\boldsymbol{\sigma}\left(\mathbf{u}^h, D^h\right)$ at $t^{(k+1)}$. The stress state evaluation is achieved by discretizing the evolution equations of the stress and damage together with the consistency conditions

$$Y\left(\mathbf{x}, t^{(k+1)}\right) - \omega\left(\boldsymbol{\theta}, D\left(\mathbf{x}, t^{(k+1)}\right)\right) \leq 0. \tag{19}$$

To insure the above consistency conditions, an implicit Backward Euler method is utilized here. In this regard, the incremental value of the damage variable can be obtained using the Newton iterative procedure (see [4] for more details).

3 The Dynamic Data Driven Application System

As a prototypical problem of composite damage evolution, in this study a sheet of a carbon-fiber epoxy composite is considered that is commonly used in aerospace applications. The specimen is subjected to a monotonically increasing load or load-unload cycles with increasing load up to failure [4]. At different stages in this process, the specimen is interrogated in order to determine the spatial variation in the strain using digital image correlation and map this to damage.

The Dynamic Data Driven control system is depicted in Figure 1. The dotted lines indicate that the statistically inferred state of the material can be used to drive a variety of actions. Here "state" refers to a joint probability density function (PDF) of the material parameters and the damage field. Possible data driven actions are mesh refinement (mesh is refined around regions of increasing damage), load control, healing control, and measurement control (measurements become concentrated in regions of increasing damage).

There are two main computational cycles in the control system depicted in Figure 1. One computational cycle involves "only" simulations, and is responsible for predicting the state. Beginning with an initial state (one usually assumes that no damage exists), the computational model is exercised during the solution of the statistical forward problem for one time step. While experimental data is not yet available, the predicted state feeds back through the statistical forward problem, so that the state can be predicted at the next time step. Eventually, the mesh may need to be refined to predict the state more accurately.

The other computational cycle in Figure 1 involves a Bayesian updating procedure, and is responsible for dynamically updating our knowledge about the state, as data is collected. Once experimental data is accessed at a particular time, it can be used to update our knowledge about the system state, using prior knowledge (predicted state) to gain posterior knowledge (corrected state). The computational model and the experimental data are used in the computation of the likelihood function in Bayes' formula (see Section 5). The corrected damage state is then fed back to the forward problem as time is advanced and the loop begins again. Local mesh refinement may be required at this point to capture the damage interface with sufficient accuracy. This is indicated by the dotted line at the top of Figure 1. The corrected damage state might also drive other control actions, as indicated by the three dotted lines on the bottom of Figure 1. For instance, in cases in which the material is part of a structural component in service, possible actions might be: (i) to instantly apply healing (an example of control) to a damaged region, and/or (ii) to instantly update a flight

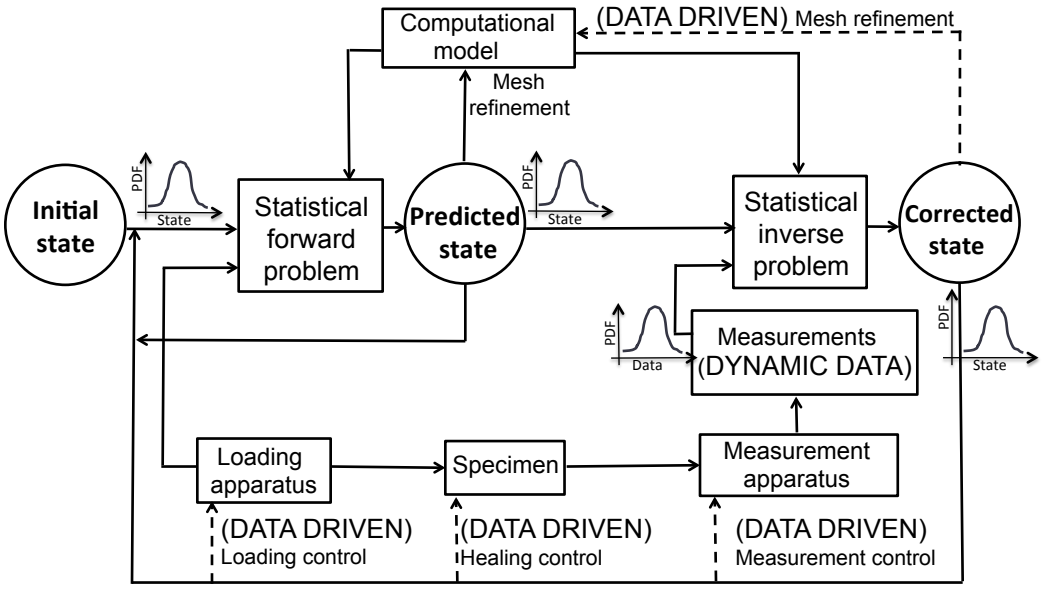

Figure 1: A schematic representation of the DDDAS. Here "state" refers to the combination of physical parameters and the scalar damage field throughout the specimen. The four dotted lines highlight the possible (dynamic) data driven actions.

maneuver plan (another example of control) in order to diminish the possibility that any further damage happens to the system, and/or (iii) update the flight computer so that it has up-to-date information before taking a maneuver decision.

It is important to note that many uncertainties are involved in the process of assessing the system state: the data is measured only at some points of the system, the measured data has noise, the computational model that maps the spatial distribution of damage to the spatial distribution of strain (or electric potential) is an imperfect characterization of reality, and the damage evolution model may not capture reality perfectly either. All these uncertainties justify the use of statistical problems in Figure 1.

4 Experimental Observations

In order to provide experimental evidence for conducting statistical calibration, validation and selection of the continuum damage models, a set of experimental data are dynamically recorded for a polymer nano-composite material, see [4]. This experimental work involves uniaxial tensile experiments with different load levels for measuring strain variation over the length of the specimens, and for generating distributed damage in different parts of the specimen. Moreover, in order to provide for real-time monitoring of damage, [4] postulated a second group of experiments for dynamically and indirect measuring local variation of damage along the length of the specimen. In the experiment reported in [4], the specimens are made of a bisphenol A epoxy resin infused with multiwalled carbon nanotubes (CNTs) dispersed uniformly through the specimen. The presence of the CNTs makes the specimen electrically conductive and provides the possibility of determining the damage state through

electrical conductivity measurements. These specimens are subjected to loading-unloading cycles with progressively increasing peak displacements between two rigid cross-heads in a testing machine. The global response of the specimen is characterized easily by measuring the force and extension; the variation of the nominal stress (load/original area) with average global strain is shown in Figure 2(a). The spatial variation in the strain field (resulting from local perturbations in material state and properties) is also measured at each load increment using digital image correlation. Moreover, the spatial variation of electrical conductivity (averaged across the width of the specimen) is measured using a four-point conductivity probe at a selected number of positions along the length of the specimen. The connection between the conductivity changes and damage in term of micro-cracks can provide an indirect measurement of damage. However, observations of [4] suggest that the underlying mechanisms that dictate the changes in resistance with position, strain and stress, as well as time-dependence are quite complex and may require a more in-depth examination before the CNT infiltrated epoxies can be used as diagnostic sensors. Therefore, in the current work, the results of the indirect measurement of damage is not considered for the statistical analyses.

4.1 Experimental Characterization of the Variation of Strain

Figure 2(b) shows a contour plot corresponding to the strain, ϵ at a particular step in the loading process when the average strain in the specimen was about 1.4%. Figure 2(c) shows the variation along x, the horizontal direction, of the strain at different times after beginning of the test (particularly at one set of each unloading). This data corresponds to $u(t^{(k)}, x_i)$, the measured displacement variation along x at time (i.e. load increment) k. There are two key features that are evident; first, while the average strain is about 1.4%, there is a background fluctuation over the entire length that arises from the noise in the process of digital image correlation used to evaluate the strains. Second, there are some hot-spots where the strains are quite a bit higher than the average strain; these fluctuations are well above the noise in the measurements and correspond to points in the specimen where local defects trigger damage accumulation. Eventually, one of these hot-spots results in failure of the specimen. This development of strain (or damage) accumulation is illustrated in Figure 2(d) where the variation of the strain in the uniform segment is shown in comparison to the strain in the hot-spot; rapid accumulation of strain leading up to failure of the specimen occurs in the last cycle.

The measured displacement data $u(t^{(k)}, x_i)$, and the corresponding measured force $f_{\text{exp}}(t^{(k)})$ from the lead cell for all time steps, constitutes the experimental data set $\mathbf{d}(t^{(k)}, x_i) = \left\{u(t^{(k)}, x_i), f_{\text{exp}}(t^{(k)})\right\}$ to be used in calibration of the damage model. Based on the DIC resolution, the displacement data is measured in a grid that consists of 91 evenly-spaced points along x (i.e. $0 \leq i \leq 90$) and 17 points along y. Moreover, the DIC system is set to image the specimen with the rate of 1 image per second. Considering the total time of 500(s) for conducting the test, the displacement and force are capture at 500 time steps (i.e. $0 \leq k \leq 500$).

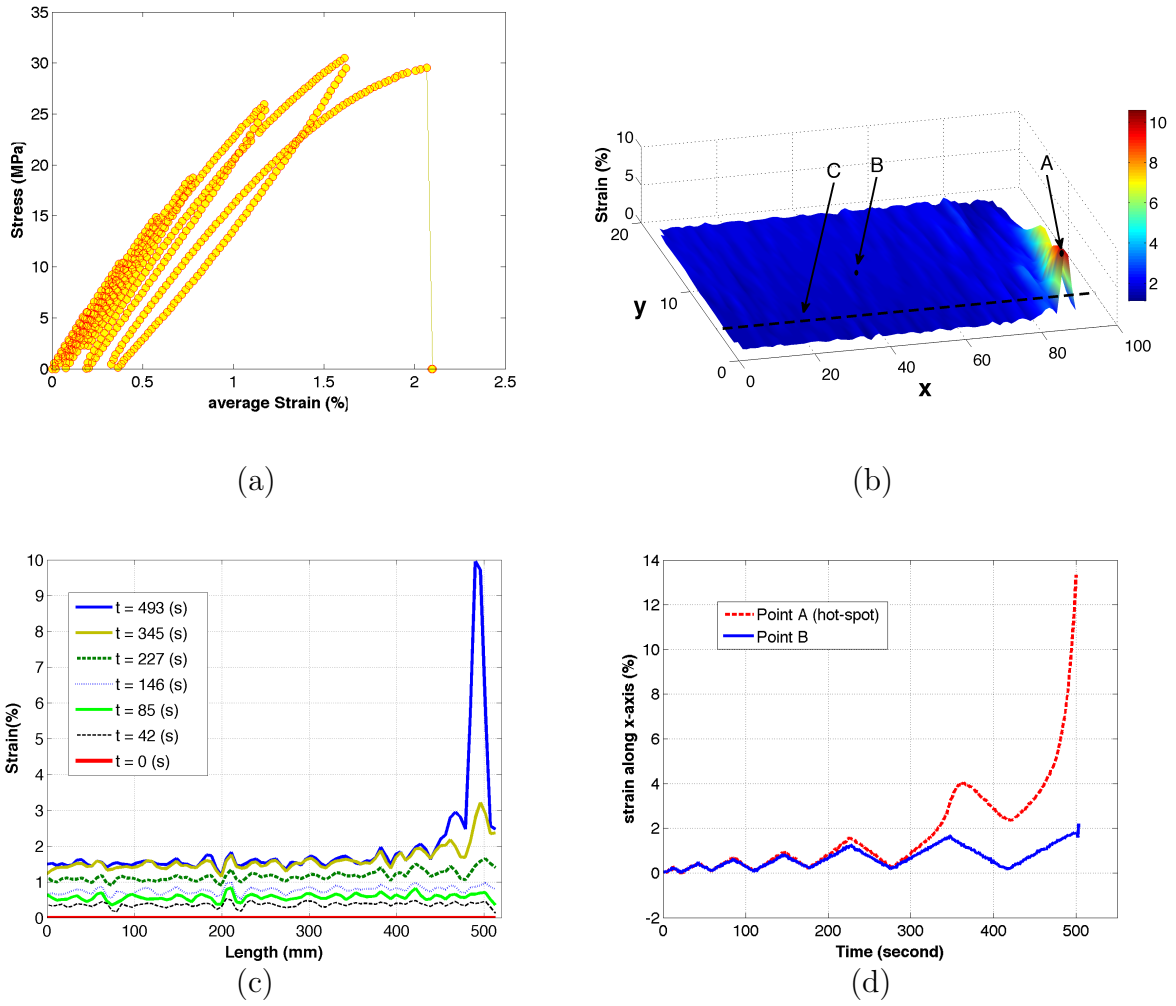

Figure 2: Experimental results of the CNT-Epoxy specimen: (a) The nominal stress vs nominal strain plot indicating the load-unload cycles that the specimen experienced; (b) Spatial variation of strain at $t = 493$(s) after beginning the test; (c) the strain variation along x (line C as shown in plot (b)) at different times (one set of unloading); (d) evolution of strain through time in the hot-spot and in the uniform segment (points A and B as shown in plot (b) respectively)[4].

5 Bayesian Analysis and Model Plausibilities

We are interested in statistically inferring the current state of a system of physical volume $\Omega \subset \mathbb{R}^3$, so that we can make predictions about the system and consequently inform the model of potential control actions to be taken, given our updated knowledge about its state. For instance, the state might be the set of physical parameter values. The state will be indicated by the vector $\boldsymbol{\theta} \in \mathbb{R}^{n_\theta}$, for some fixed positive integer $n_\theta > 0$. In order to proceed with the state inference, we collect measurement data $\mathbf{d} \in \mathbb{R}^{n_d}$, for some fixed positive integer $n_d > 0$. Our current (pre-inference), and uncertain knowledge of the system state is represented by the prior probability density function $\pi_{\text{prior}}(\boldsymbol{\theta})$. The posterior (post-inference)

state is given by Bayes' formula [19]:

$$\pi_{\text{post}}(\boldsymbol{\theta}|\mathbf{d}) = \frac{\pi_{\text{like}}(\mathbf{d}|\boldsymbol{\theta}) \cdot \pi_{\text{prior}}(\boldsymbol{\theta})}{\pi_{\text{data}}(\mathbf{d})}. \tag{20}$$

In (20), $\pi_{\text{post}}(\boldsymbol{\theta}|\mathbf{d})$ is the posterior PDF defining the Bayesian update of the prior information embodied in $\pi_{\text{prior}}(\boldsymbol{\theta})$. The likelihood PDF, $\pi_{\text{like}}(\mathbf{d}|\boldsymbol{\theta})$, encapsulates assumptions about the discrepancy between the values $\mathbf{d}$ that are measured and the values that can be computed with the computational model we have at our disposal. And the term

$$\pi_{\text{data}}(\mathbf{d}) = \int \pi_{\text{like}}(\mathbf{d}|\boldsymbol{\theta}) \cdot \pi_{\text{prior}}(\boldsymbol{\theta}) \, d\boldsymbol{\theta}$$

is the normalization value (for a given $\mathbf{d}$) that makes (20) a PDF.

For the DDDAS of interest here:

- Ω = some material piece that might be subjected to stresses and consequent damages;
- $\mathbf{d}$ = strain (or electrical resistivity) measured at n_d positions of the system; and
- $\boldsymbol{\theta}$ = parameters of the damage constitutive material model(s) (a vector of size n_θ) inferred by statistical inversion.

Once we infer such spatial distributions, the control decision might be (in case the material is part of an airplane in service, for example):

- to instantly apply healing (an example of control) to a damaged region, and/or
- to instantly update a loading scenario of the structure (another example of control) in order to diminish the possibility that any further damage happens to the system, and/or
- update sensor control of the structural system so that it has up-to-date information before implementing a control decision.

However, many uncertainties are involved in the process of assessing the system state:

- the data is measured only at some points of the system,
- the measured data has noise,
- the continuum damage mechanics models do not capture real responses of the material perfectly, and
- the computational model that maps the spatial distribution of resistivity to the spatial distribution of damage is an imperfect characterization of reality.

5.1 Model Plausibilities

Formula (20) can also be written to make explicit the whole set of assumptions underlying the modeling and inference efforts [8, 29, 28]:

$$\pi_{\text{post}}(\boldsymbol{\theta_j}|\mathbf{d}, M_j) = \frac{\pi_{\text{like}}(\mathbf{d}|\boldsymbol{\theta_j}, M_j) \cdot \pi_{\text{prior}}(\boldsymbol{\theta_j}|M_j)}{\pi_{\text{data}}(\mathbf{d}|M_j)}. \tag{21}$$

In (21), M_j denotes the j-th model class, which has associated with it a random vector $\boldsymbol{\theta_j}$ of model parameters, $j = 1, 2, \ldots, m$. All m proposed model classes are "competing" to explain (match) the same collected data $\mathbf{d}$. Any arbitrarily fixed parameter sample $\boldsymbol{\theta_j}^*$ in M_j is called a model. That is, a model class can be seen as the family of all possible values of $\boldsymbol{\theta_j}$, augmented with prior and likelihood PDFs. It should be noted that different model classes might have different parameters.

In (21), the term

$$\pi_{\text{data}}(\mathbf{d}|M_j) = \int \pi_{\text{like}}(\mathbf{d}|\boldsymbol{\theta_j}, M_j) \cdot \pi_{\text{prior}}(\boldsymbol{\theta_j}|M_j)\ d\boldsymbol{\theta_j} \tag{22}$$

is denoted "model evidence", and it reflects how likely one is to obtain a given data sample $\mathbf{d}$ with the whole family of models $\boldsymbol{\theta_j}$ in M_j. The model evidence can be used to update the ranking of model classes. Indeed, in the set $\mathcal{M} = \{M_1, \ldots, M_m\}$ of competing model classes, let us say that we have an a priori plausibility $\rho_{\text{prior}}(M_j|\mathcal{M})$ for each model class, with the constraint

$$\sum_{j=1}^{m} \rho_{\text{prior}}(M_j|\mathcal{M}) = 1.$$

Once we collect new data, we can update such a priori ranking (Figure 3). The posterior plausibility $\rho_{\text{post}}(M_j|\mathbf{d}, \mathcal{M})$ for each model class is also computed through a Bayesian updating procedure:

$$\rho_{\text{post}}(M_j|\mathbf{d}, \mathcal{M}) = \frac{\pi_{\text{data}}(\mathbf{d}|M_j, \mathcal{M}) \cdot \rho_{\text{prior}}(M_j|\mathcal{M})}{\pi_{\text{data}}(\mathbf{d}|\mathcal{M})}. \tag{23}$$

In (23), the term

$$\pi_{\text{data}}(\mathbf{d}|\mathcal{M}) = \sum_{j=1}^{m} \pi_{\text{data}}(\mathbf{d}|M_j, \mathcal{M}) \cdot \rho_{\text{prior}}(M_j|\mathcal{M})$$

is the normalization value (for a given $\mathbf{d}$) that makes (23) a probability mass function (PMF)(note the use of "ρ" instead of "π"). It reflects how likely one is to obtain a given data sample $\mathbf{d}$ with the whole family of model classes M_j in $\mathcal{M}$.

In this work, we will make use (21) and (23) in order to calibrate and rank some of the models of Section 2. For instance, $\boldsymbol{\theta_1} = (E, s, \epsilon_{\text{R}})$ for the Krajcinovic model (4) and $\boldsymbol{\theta_2} = (E, \alpha, \beta)$ for the Marigo model (5).

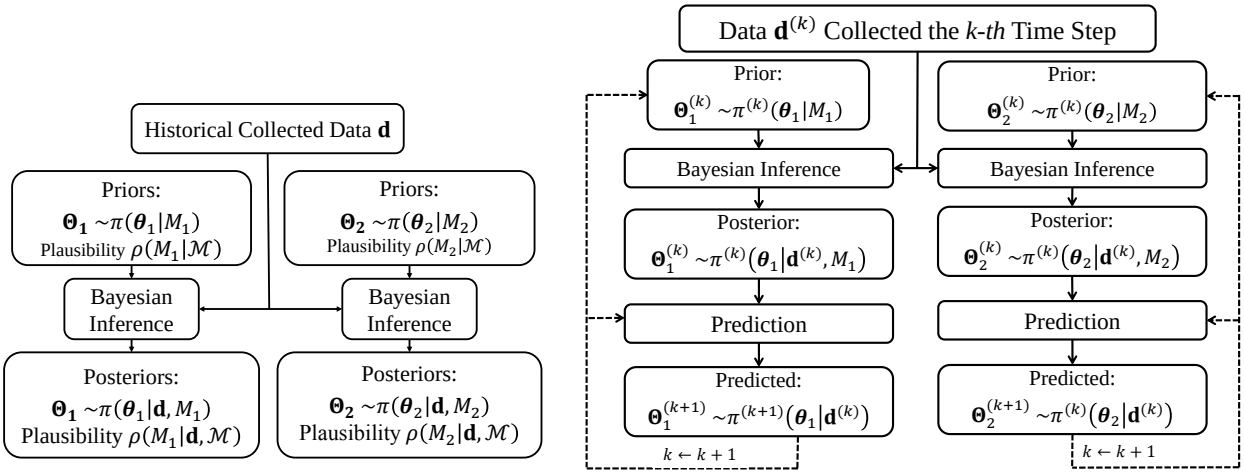

Figure 3: Model plausibilities algorithms: (a) Batch inference; (b) Real time inference.

5.2 The General Bayesian Filtering

We now explore the statistical assessment of how the system state evolves with time $t \in [0, +\infty)$, so that the model can be informed of potential decisions to be taken about the system, and/or potential control actions to be taken. For instance, the state might be a scalar damage field throughout a volume region. The initial state of the system is specified by the PDF $\pi(\boldsymbol{\theta}^{(0)})$. The (eventual) control will be indicated by the vector $\mathbf{c} \in \mathbb{R}^{n_c}$, for some fixed positive integer $n_c > 0$. In order to assess the system state, we collect measurement data $\mathbf{d}^{(1)}$, $\mathbf{d}^{(2)}, \ldots$, at instants $0 = t^{(0)} < t^{(1)} < t^{(2)} < \ldots$, and then apply Bayes' formula

$$\pi_{\text{post}}(\boldsymbol{\theta}^{(k)}|\mathbf{d}^{(k)}) = \frac{\pi_{\text{like}}(\mathbf{d}^{(k)}|\boldsymbol{\theta}^{(k)}) \cdot \pi_{\text{prior}}(\boldsymbol{\theta}^{(k)})}{\pi_{\text{data}}(\mathbf{d}^{(k)})}. \tag{24}$$

If no control is applied, or if we believe that the state should remain unchanged, Bayes' formula (24) is applied every time new data is collected, in order to update our knowledge about the system state. Implicit in this understanding is the equality

$$\pi_{\text{prior}}(\boldsymbol{\theta}^{(k+1)}) = \pi_{\text{post}}(\boldsymbol{\theta}^{(k)}|\mathbf{d}^{(k)}).$$

However, if control is applied, or if we believe the state changes over time due to events beyond our control, then:

(a) [Prediction step] One might need to use an evolution equation in order to predict the state of the system. A possible discrete form of such evolution equation is

$$\boldsymbol{\theta}^{(k+1)} = \mathbf{f}^{(k+1)}(\boldsymbol{\theta}^{(k)}, \mathbf{c}^{(k+1)}, \mathbf{w}^{(k)}), \tag{25}$$

where $\mathbf{f}^{(k+1)}(\cdot, \cdot, \cdot)$ is an evolution function and $\mathbf{w}$ denotes the state noise. Once the new state $\boldsymbol{\theta}^{(k+1)}$ is predicted, one can also predict the next measurement to be obtained at $t^{(k+1)}$. A possible discrete form of such prediction is given by the output equation

$$\mathbf{y}^{(k+1)} = \mathbf{g}^{(k+1)}(\boldsymbol{\theta}^{(k+1)}, \mathbf{v}^{(k+1)}), \tag{26}$$

where $\mathbf{g}^{(k+1)}(\cdot, \cdot)$ is an output function and $\mathbf{v}$ denotes the output noise;

(b) [Correction step] Then, finally, one can actually measure data $\mathbf{d}^{(k+1)}$ at $t^{(k+1)}$. The comparison between the model output $\mathbf{y}^{(k+1)}$ and the measurements $\mathbf{d}^{(k+1)}$ in the likelihood PDF will then allow one to statistically update the predicted state $\boldsymbol{\theta}^{(k+1)}$ using Bayes' formula (24).

The steps (a)-(b) continue as long as we want to assess and control the state of our system (Figure 4).

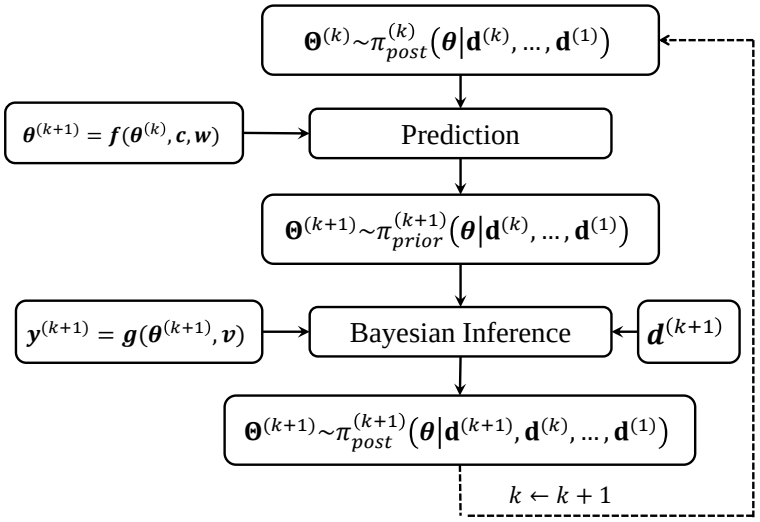

Figure 4: General Bayesian filtering algorithm.

Such continuing process can be represented by the equation

$$\pi_{\text{post}}(\boldsymbol{\theta}^{(k+1)}|\mathbf{d}^{(k+1)}, \mathbf{d}^{(k)}, \ldots, \mathbf{d}^{(1)}) = \frac{\pi_{\text{like}}(\mathbf{d}^{(k+1)}, \mathbf{d}^{(k)}, \ldots, \mathbf{d}^{(1)}|\boldsymbol{\theta}^{(k+1)}) \cdot \pi_{\text{prior}}(\boldsymbol{\theta}^{(k+1)})}{\pi_{\text{data}}(\mathbf{d}^{(k+1)}, \mathbf{d}^{(k)}, \ldots, \mathbf{d}^{(1)})}. \quad (27)$$

If one assumes (i) that the system state follows a first-order Markov process, that is,

$$\pi_{\text{state}}(\boldsymbol{\theta}^{(k+1)}|\boldsymbol{\theta}^{(k)}, \ldots, \boldsymbol{\theta}^{(0)}) = \pi_{\text{state}}(\boldsymbol{\theta}^{(k+1)}|\boldsymbol{\theta}^{(k)}), \quad (28)$$

and (ii) that, given a current state, the measurements are independent of previous measurements, that is,

$$\pi_{\text{like}}(\mathbf{d}^{(k+1)}|\mathbf{d}^{(k)}, \ldots, \mathbf{d}^{(1)}, \boldsymbol{\theta}^{(k+1)}) = \pi_{\text{like}}(\mathbf{d}^{(k+1)}|\boldsymbol{\theta}^{(k+1)}), \quad (29)$$

then (27) can be rewritten as [18, 20, 32]

$$\pi_{\text{post}}(\boldsymbol{\theta}^{(k+1)}|\mathbf{d}^{(k+1)}, \mathbf{d}^{(k)}, \ldots, \mathbf{d}^{(1)}) = \frac{\pi_{\text{like}}(\mathbf{d}^{(k+1)}|\boldsymbol{\theta}^{(k+1)}) \cdot \pi_{\text{prior}}(\boldsymbol{\theta}^{(k+1)}|\mathbf{d}^{(k)}, \ldots, \mathbf{d}^{(1)})}{\pi_{\text{data}}(\mathbf{d}^{(k+1)}|\mathbf{d}^{(k)}, \ldots, \mathbf{d}^{(1)})}. \quad (30)$$

In (30), the term

$$\pi_{\text{prior}}(\boldsymbol{\theta}^{(k+1)}|\mathbf{d}^{(k)}, \ldots, \mathbf{d}^{(1)}) = \int \pi_{\text{state}}(\boldsymbol{\theta}^{(k+1)}|\boldsymbol{\theta}^{(k)}, \mathbf{d}^{(k)}, \ldots, \mathbf{d}^{(1)}) \cdot \pi_{\text{post}}(\boldsymbol{\theta}^{(k)}|\mathbf{d}^{(k)}, \ldots, \mathbf{d}^{(1)})\, d\boldsymbol{\theta}^{(k)}$$

involves the evolution Equation (25), while the term

$$\pi_{\text{like}}(\mathbf{d}^{(k+1)}|\boldsymbol{\theta}^{(k+1)})$$

involves the output Equation (26). The recursive nature of (30) is clear, in the sense that one makes the transition

$$\pi_{\text{post}}(\boldsymbol{\theta}^{(k)}|\mathbf{d}^{(k)},\ldots,\mathbf{d}^{(1)}) \quad \longrightarrow \quad \pi_{\text{post}}(\boldsymbol{\theta}^{(k+1)}|\mathbf{d}^{(k+1)},\mathbf{d}^{(k)},\ldots,\mathbf{d}^{(1)}). \tag{31}$$

The PDF transition (31) can be broken into two intermediate transitions, namely the prediction and correction steps mentioned above. The prediction step relates itself to the PDF transition

$$\pi_{\text{post}}(\boldsymbol{\theta}^{(k)}|\mathbf{d}^{(k)},\ldots,\mathbf{d}^{(0)}) \quad \longrightarrow \quad \pi_{\text{prior}}(\boldsymbol{\theta}^{(k+1)}|\mathbf{d}^{(k)},\ldots,\mathbf{d}^{(0)}), \tag{32}$$

while the correction step relates itself to the PDF transition

$$\pi_{\text{prior}}(\boldsymbol{\theta}^{(k+1)}|\mathbf{d}^{(k)},\ldots,\mathbf{d}^{(0)}) \quad \longrightarrow \quad \pi_{\text{post}}(\boldsymbol{\theta}^{(k+1)}|\mathbf{d}^{(k+1)},\mathbf{d}^{(k)},\ldots,\mathbf{d}^{(0)}). \tag{33}$$

The Bayesian filtering procedure (30) is usually intractable computationally. However, it can be simplified with further assumptions, as discussed in the next two subsections. Before proceeding, though, we list two extra important notations. Given a PDF $\pi(\boldsymbol{\theta})$, we will denote by

$$\hat{\boldsymbol{\theta}} = \arg\max_{\boldsymbol{\theta}} \quad \pi(\boldsymbol{\theta}), \tag{34}$$

a Maximum a Posteriori (MAP) Estimation. Also, we will denote by $\mathcal{N}(\boldsymbol{\mu},\mathbf{C})$ a (multivariate) Gaussian distribution of mean $\boldsymbol{\mu}$ and (co)variance (matrix) $\mathbf{C}$.

It should be noted that hypotheses (28) and (29) are always assumed to be valid throughout this article.

5.3 The Kalman Filter

Let us first assume the model allows for linearization in which the aforementioned Bayesian filtering procedure can be reduced into the Kalman filter. Moreover, suppose the following five assumptions hold $\forall\ k \geqslant 0$, for known vector $\hat{\boldsymbol{\theta}}^{(0)}$, as well as known matrices $\mathbf{A}^{(k+1)}$, $\mathbf{B}^{(k+1)}$, $\mathbf{H}^{(k+1)}$, $\mathbf{P}^{(0)}$, $\mathbf{Q}^{(k)}$, and $\mathbf{R}^{(k+1)}$:

$$\begin{aligned}
\mathbf{f}^{(k+1)}(\boldsymbol{\theta}^{(k)},\mathbf{u}^{(k+1)},\mathbf{w}^{(k)}) &= \mathbf{A}^{(k+1)}\cdot\boldsymbol{\theta}^{(k)} + \mathbf{B}^{(k+1)}\cdot\mathbf{u}^{(k+1)} + \mathbf{w}^{(k)}, && (35)\\
\mathbf{g}^{(k+1)}(\boldsymbol{\theta}^{(k+1)},\mathbf{v}^{(k+1)}) &= \mathbf{H}^{(k+1)}\cdot\boldsymbol{\theta}^{(k+1)} + \mathbf{v}^{(k+1)}, && (36)\\
\boldsymbol{\theta}^{(0)} &\sim \mathcal{N}(\hat{\boldsymbol{\theta}}^{(0)},\mathbf{P}^{(0)}), && (37)\\
\mathbf{w}^{(k)} &\sim \mathcal{N}(\mathbf{0},\mathbf{Q}^{(k)}),\ \text{and} && (38)\\
\mathbf{v}^{(k+1)} &\sim \mathcal{N}(\mathbf{0},\mathbf{R}^{(k+1)}), && (39)
\end{aligned}$$

where $\mathbf{A}$ describes how state evolves from $t^{(k)}$ to $t^{(k+1)}$, $\mathbf{B}$ describes how control changes the state from $t^{(k)}$ to $t^{(k+1)}$, and $\mathbf{H}$ describes how to map the state $\boldsymbol{\theta}$ to an observation $\mathbf{y}$ (see (26)).

Then the general process (30) can be substituted by the following five steps, assuming that $\hat{\boldsymbol{\theta}}^{(k)}$, $\mathbf{P}^{(k)}$ and $\mathbf{d}^{(k+1)}$ are known:

$$\tilde{\boldsymbol{\theta}}^{(k+1)} = \mathbf{A}^{(k+1)} \cdot \hat{\boldsymbol{\theta}}^{(k)} + \mathbf{B}^{(k+1)} \cdot \mathbf{u}^{(k+1)}, \tag{40}$$

$$\tilde{\mathbf{P}}^{(k+1)} = \mathbf{A}^{(k+1)} \cdot \mathbf{P}^{(k)} \cdot \mathbf{A}^{(k+1)^T} + \mathbf{Q}^{(k)}, \tag{41}$$

$$\mathbf{K}^{(k+1)} = \tilde{\mathbf{P}}^{(k+1)} \cdot \mathbf{H}^{(k+1)^T} \cdot \left(\mathbf{H}^{(k+1)} \cdot \tilde{\mathbf{P}}^{(k+1)} \cdot \mathbf{H}^{(k+1)^T} + \mathbf{R}^{(k+1)} \right)^{-1}, \tag{42}$$

$$\hat{\boldsymbol{\theta}}^{(k+1)} = \tilde{\boldsymbol{\theta}}^{(k+1)} + \mathbf{K}^{(k+1)} \cdot \left(\mathbf{d}^{(k+1)} - \mathbf{H}^{(k+1)} \cdot \tilde{\boldsymbol{\theta}}^{(k+1)} \right), \text{ and} \tag{43}$$

$$\hat{\mathbf{P}}^{(k+1)} = \left(\mathbf{I} - \mathbf{K}^{(k+1)} \cdot \mathbf{H}^{(k+1)} \right) \cdot \tilde{\mathbf{P}}^{(k+1)}. \tag{44}$$

Under the Kalman filter assumptions, the system state will always be Gaussian. So, at each time step it suffices to determine the mean (43) and the covariance (44). Substeps (40)-(41) correspond to the prediction step (32), while substeps (42)-(44) correspond to the correction step (33) (Figure 5). The matrix $\mathbf{K}$ in (42) is called the Kalman gain.

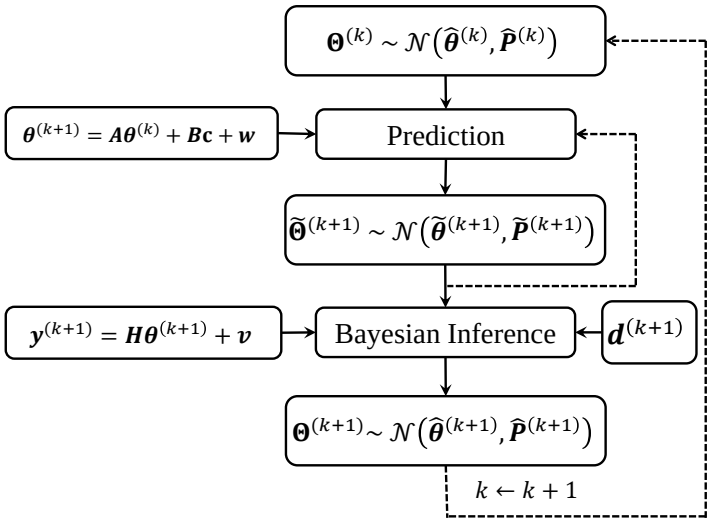

Figure 5: Kalman filtering algorithm.

5.4 The Extended Kalman Filter

In case the system is not linear nor Gaussian, one possible approach is to linearize both the evolution function $\mathbf{f}^{(k+1)}(\cdot,\cdot,\cdot)$ in (25) and the output function $\mathbf{g}^{(k+1)}(\cdot,\cdot)$ in (26). The general process (30) can then be substituted by the following five steps (Figure 6):

$$\tilde{\boldsymbol{\theta}}^{(k+1)} = \mathbf{f}^{(k+1)}(\hat{\boldsymbol{\theta}}^{(k)}, \mathbf{u}^{(k+1)}, \mathbf{0}), \tag{45}$$

$$\tilde{\mathbf{P}}^{(k+1)} = \mathbf{A}^{(k+1)} \cdot \mathbf{P}^{(k)} \cdot \mathbf{A}^{(k+1)^T} + \mathbf{W}^{(k+1)} \cdot \mathbf{Q}^{(k)} \cdot \mathbf{W}^{(k+1)^T}, \tag{46}$$

$$\mathbf{K}^{(k+1)} = \tilde{\mathbf{P}}^{(k+1)} \cdot \mathbf{H}^{(k+1)^T} \cdot \left(\mathbf{H}^{(k+1)} \cdot \tilde{\mathbf{P}}^{(k+1)} \cdot \mathbf{H}^{(k+1)^T} + \mathbf{V}^{(k+1)} \cdot \mathbf{R}^{(k+1)} \cdot \mathbf{V}^{(k+1)^T} \right)^{-1}, \tag{47}$$

$$\hat{\boldsymbol{\theta}}^{(k+1)} = \tilde{\boldsymbol{\theta}}^{(k+1)} + \mathbf{K}^{(k+1)} \cdot \left(\mathbf{d}^{(k+1)} - \mathbf{g}^{(k+1)}(\tilde{\boldsymbol{\theta}}^{(k+1)}, \mathbf{0}) \right), \text{ and} \tag{48}$$

$$\hat{\mathbf{P}}^{(k+1)} = \left(\mathbf{I} - \mathbf{K}^{(k+1)} \cdot \mathbf{H}^{(k+1)} \right) \cdot \tilde{\mathbf{P}}^{(k+1)}, \tag{49}$$

where

$$\mathbf{A}_{ij}^{(k+1)} = \frac{\partial \mathbf{f}_i^{(k+1)}}{\partial \theta_j}(\hat{\boldsymbol{\theta}}^{(k)}, \mathbf{u}^{(k+1)}, \mathbf{0}), \tag{50}$$

$$\mathbf{W}_{ij}^{(k+1)} = \frac{\partial \mathbf{f}_i^{(k+1)}}{\partial w_j}(\hat{\boldsymbol{\theta}}^{(k)}, \mathbf{u}^{(k+1)}, \mathbf{0}), \tag{51}$$

$$\mathbf{H}_{ij}^{(k+1)} = \frac{\partial \mathbf{g}_i^{(k+1)}}{\partial \theta_j}(\tilde{\boldsymbol{\theta}}^{(k+1)}, \mathbf{0}), \tag{52}$$

and

$$\mathbf{V}_{ij}^{(k+1)} = \frac{\partial \mathbf{g}_i^{(k+1)}}{\partial v_j}(\tilde{\boldsymbol{\theta}}^{(k+1)}, \mathbf{0}). \tag{53}$$

Above, obviously, it is assumed that one knows $\hat{\boldsymbol{\theta}}^{(0)}$, $\mathbf{P}^{(0)}$, $\mathbf{Q}^{(k)}$, and $\mathbf{R}^{(k+1)}$, $\forall\ k \geqslant 0$.

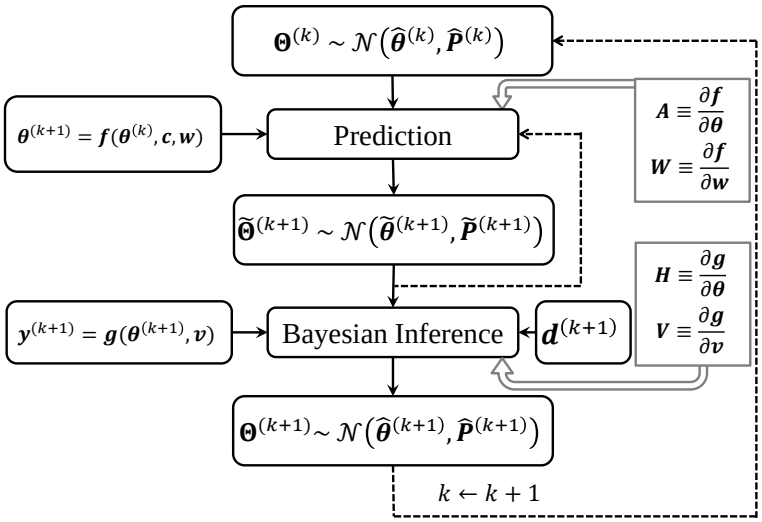

Figure 6: Extended Kalman filtering algorithm.

6 Implementation Aspects and Integration

To implement the DDDAS, the mathematical model for continuum damage mechanics, the Kalman filter algorithm, and the generated experimental data are integrated into a cohesive infrastructure. Software modules incorporated in the analysis system are indicated in Figure 7. The DDDAS is built on the software systems QUESO[1] [30], libMesh[2] [22], PETSc [2, 1, 3], GSL, BOOST, and STL.

[1]Quantification of Uncertainty for Estimation, Simulation and Optimization (QUESO) is a collection of C++ classes and algorithms to support model validation and the prediction of quantities of interest with uncertainty quantification (UQ) included [17].

[2]The libMesh library provides a framework for the numerical simulation of partial differential equations particularly for adaptive mesh refinement computations using arbitrary unstructured discretizations on serial and parallel platforms.

The statistical inverse problem and statistical forward are conducted using parallel MPI /C++ software libraries QUESO. A likelihood function and a quantity of interest function (QoI) must be specified in the statistical inverse and forward problems. QUESO provides tools for both sampling algorithms for statistical inverse problems, following Bayes' formula, and statistical forward problems. One of the most challenging parts in the implementation of Bayesian methodologies is the evaluation of integrals such as (22). QUESO make use of Markov Chain Monte Carlo (MCMC) algorithms for sampling posterior PDFs and evaluating integrals, and then Monte Carlo algorithms for sampling Quantity of Interest (QoI) PDFs (as well as evaluating integrals), usually in combination with high-performance computing. However, a naive application of MCMC algorithm can lead to poor estimates of integral, since some modes of the posterior PDF might be missed. One simple idea to improve the chances of exploring all existing modes, and therefore computing good estimates for the integrals, is to sample increasingly difficult intermediate distributions, accumulating information from one intermediate distribution to the next, until the target posterior distribution is better sampled. Possible intermediate distributions are given by [29]:

$$\pi_{\text{int}}^{(\ell)}(\boldsymbol{\theta}_j|\mathbf{d}, M_j) = [\pi_{\text{like}}(\mathbf{d}|\boldsymbol{\theta}_j, M_j)]^{\alpha_\ell} . \pi_{\text{prior}}(\boldsymbol{\theta}_j|M_j), \quad \ell = 0, 1, \cdots, L, \tag{54}$$

for a given $L > 0$ and a sequence $0 = \alpha_0 < \alpha_1 < \ldots < \alpha_L = 1$ where $\alpha_\ell = 0$ and $\alpha_\ell = 1$ denote the prior and posterior distribution respectively. Therefore as ℓ increases, the distribution transitions from the initial prior to the (eventually multimodal) posterior. Such sampling algorithms can greatly benefit from parallel computing. For more information see [29].

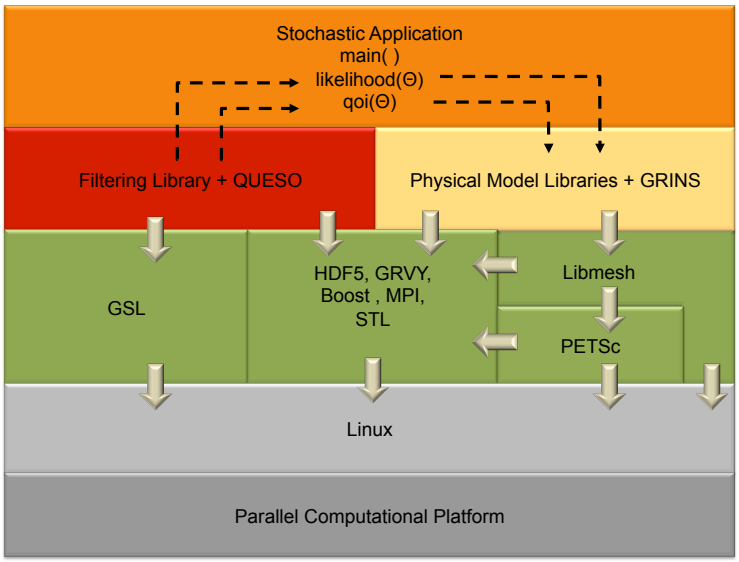

Figure 7: The software stack related to

Moreover, in this study the Kalman filtering, as well as the extended Kalman filtering (as formulated in Section 5) are applied to the software libraries QUESO [30].

In this work, the libMesh library is used for a parallel, C++ finite element implementation of the damage model described in Section 2. Through libMesh, we also leveraged the well established linear and nonlinear solver packages, such as PETSc, to solve the resulting systems of equations that arise in the damage model.

The other code in Figure 7, referred to as Top Application, deals with the definition of statistical inverse problems (parameter spaces, prior PDFs, likelihood functions, reference data), as well as with the proper use of QUESO C++ classes in order to solve such statistical inverse problems through Bayesian formula and Markov Chain Monte Carlo (MCMC) algorithms, and in order to calculate evidences and other integrals. Parallel computing is used in all computational steps.

7 Results

7.1 Statistical Calibration and Plausibility of Damage Models

7.1.1 General consideration

Throughout the Section 4 the physical domain corresponding to the size of the high spatial resolution images is the rectangle $\Omega_{\text{actual}} = (0, 51.29) \times (0, 9.68)$ millimeters. In order to diminish the computational cost, we solved only for the center line $\Omega = (0, 51.29) \times (4.81, 4.81)$ with averaging the strain measurements through the width of the specimen. As is explained in Section 2, we disceretized the the equations in space with a finite element mesh, and in time with an explicit time stepping scheme with a fixed time step[3] Δt.

In order to conduct the calibration and compute the evidences, one has to decide on the following:

- damage model(s) to be considered;
- what form of likelihood is to be taken into account;
- which parameters are to be treated as random variable (instead of deterministic);
- what prior PDFs are to be use for the random parameters (e.g. uniform distribution, Gaussian distribution); and

For the choice of damage model, among the ones mentioned in Section 2, we selected the Krajcinovic (M_1) and Marigo (M_2) damage models. The other aforementioned decisions will be illustrated below.

7.1.2 The likelihood

The form of the likelihood function reflects the way the discrepancy between the quantities computed with the material constitutive relation and the reference data is modeled. As

[3]Parallel computing is used in all computational steps. More specifically, we took advantageous of Lonestar computational platform at the Texas Advanced Computing Center (TACC [31]), where each computational node contains 24 GB of memory and 12 processing cores of 2GHz each.

indicated previously, the reference data $\mathbf{d}$ provided through the experiment consist of the measured displacement variation along $\mathbf{x}$ and force at each time step. It is known that such data are measured only at some points of the system and is contaminated with noise (i.e. error in data). Moreover, the continuum damage models are imperfect characterization of reality (i.e. error in model). In order to account for such uncertainties in both models and reference data for displacement and force, the following assumptions are made:

- The actual (and unknown) spatial distribution of displacement and force values through time $u_{\text{actual}}(t^{(k)}, x_i)$ and $f_{\text{actual}}(t^{(k)})$ are random variables corresponding to the experimental data $u_{\text{exp}}(t^{(k)}, x_i)$ and $f_{\text{exp}}(t^{(k)})$ with additional (measurement) noises $\mathbf{v}_{\text{data(displ)}}$ and $\mathbf{v}_{\text{data(load)}}$. The error in data $\mathbf{v}_{\text{data(displ)}}$ and $\mathbf{v}_{\text{data(load)}}$ are Gaussian random variables of mean 0 and (unknown) variances $\sigma_{\text{data(displ)}}$ and $\sigma_{\text{data(load)}}$, thus

$$\mathbf{v}_{\text{data(load)}} \sim \mathcal{N}(\mathbf{0}_{N_t \times 1}, \sigma^2_{\text{data(load)}} \cdot \mathbf{I}_{N_t \times N_t})$$

$$\mathbf{v}_{\text{data(displ)}} \sim \mathcal{N}(\mathbf{0}_{N_t N_x \times 1}, \sigma^2_{\text{data(displ)}} \cdot \mathbf{I}_{N_t N_x \times N_t N_x})$$

  where N_t is the number of time steps and N_x is the number of position along x.

- The actual (and unknown) spatial distribution of displacement and force values through time $u_{\text{actual}}(t^{(k)}, x_i)$ and $f_{\text{actual}}(t^{(k)})$ are random variables corresponding to the model output $u_{\text{model}}(t^{(k)}, x_i)$ and $f_{\text{model}}(t^{(k)})$ with additional (output) noises $\mathbf{v}_{\text{model(displ)}}$ and $\mathbf{v}_{\text{model(load)}}$. The error in model $\mathbf{v}_{\text{model(displ)}}$ and $\mathbf{v}_{\text{model(load)}}$ are Gaussian random variables of mean 0 and (unknown) variances $\sigma_{\text{model(displ)}}$ and $\sigma_{\text{model(load)}}$, thus

$$\mathbf{v}_{\text{model(load)}} \sim \mathcal{N}(\mathbf{0}_{N_t \times 1}, \sigma^2_{\text{model(load)}} \cdot \mathbf{I}_{N_t \times N_t})$$

$$\mathbf{v}_{\text{model(displ)}} \sim \mathcal{N}(\mathbf{0}_{N_t N_x \times 1}, \sigma^2_{\text{model(displ)}} \cdot \mathbf{I}_{N_t N_x \times N_t N_x})$$

Considering the aforementioned, one can write:

$$\sigma^2_{\text{load}} = \sigma^2_{\text{model(load)}} + \sigma^2_{\text{data(load)}},$$

$$\sigma^2_{\text{displ}} = \sigma^2_{\text{model(displ)}} + \sigma^2_{\text{data(displ)}}.$$

Therefore the form of likelihood can be postulated as

$$\begin{aligned}
\ln(\pi_{\text{like}}(\mathbf{d}|\boldsymbol{\theta_j}, M_j)) &= \frac{1}{2}\ln(2\pi) - N_t \ln(\sigma_{\text{load}}) - N_t N_x \ln(\sigma_{\text{displ}}) + \\
&- \frac{1}{2}\sum_{k=1}^{N_t} \left\{ \left[\frac{f_{\text{exp}}(t^{(k)}) - f_{\text{model}}(\boldsymbol{\theta_j}; t^{(k)})}{\sigma_{\text{load}}} \right]^2 + \right. \\
&\qquad \left. + \sum_{i=1}^{N_x} \left[\frac{u_{\text{exp}}(t^{(k)}, x_i) - u_{\text{model}}(\boldsymbol{\theta_j}; t^{(k)}, x_i)}{\sigma_{\text{displ}}} \right]^2 \right\},
\end{aligned}$$

where

- $N_t = 4$ = number of time steps used (instant ids 30, 140, 210, 320),
- $N_x = 91$ = number of "x" positions used,
- $f(t)$ = applied load at instant "t", and
- $u(t, x)$ = displacement of the specimen at instant "t" and position "x".

7.1.3 The Krajcinovic damage model M_1

Krajcinovic damage model M_1 uses (4) of Section 2 to simulate the evolution of the damage. We treat all the model constants as random variables. Therefore

$$\boldsymbol{\theta_1} = (E, s, \epsilon_R; \sigma_{\text{displ}}, \sigma_{\text{load}}).$$

In addition to such (physical) parameters, two random variables – so called (hyper) parameters – (σ_{displ} and σ_{load}) are identified in this problem. As shown previously in this section, these parameters can be interpreted as a measure of the overall discrepancy between the measured load and displacement and the corresponding quantities computed with the damage models.

The average stress-strain response gives a notation regarding the proper range of each material parameter of M_1 . We assume a uniform prior PDF for the material parameters over these ranges. Therefore, $\mathcal{U}\left((0.5e9, 0.5e10) \times (-1, 10) \times (0.001, 1)\right)$ for (E, s, ϵ_R) is presumed here where $\mathcal{U}\left(B\right)$ stands for a uniform distribution over a given set B.

7.1.4 The Marigo damage model M_2

Marigo damage model M_2 uses (5) of Section 2 as the damage evolution equation, with all the damage model parameters being treated randomly besides σ_{displ} and σ_{load}. Therefore

$$\boldsymbol{\theta_2} = (E, \alpha, \beta; \sigma_{\text{displ}}, \sigma_{\text{load}}).$$

Based on the perception of the proper range of the material parameters, we assumed a uniform prior PDF $\mathcal{U}\left((0.5e9, 0.5e10) \times (0.001, 5) \times (0.5e8, 3e8)\right)$ for (E, α, β).

7.1.5 Numerical results

As indicated in Section 5, (23) provides the means to compare model class, M_j for the given set $\mathbf{d}$ of reference data and to pick the most plausible one. A model M_1 is believed to be superior over M_2 if $\pi_{\text{posterior}}(M_1|\mathbf{d}, \mathcal{M}) > \pi_{\text{posterior}}(M_2|\mathbf{d}, \mathcal{M})$. As denoted by the conditional notation, such model ranking depends upon the specific collected data. Moreover the model evidence π_{data} plays the fundamental role in ranking of model classes.

In this section, we apply the Bayesian methodology described above to the determination of the most plausible continuum damage model between two candidate models M_1 (=Krajcinovic damage model) and M_2 (=Marigo damage model), which compete to simulate the

measured data set $\mathbf{d}(t^{(k)}, x_i) = \left\{u(t^{(t)}, x_i), f_{\exp}(t^{(k)})\right\}$. The damage model ranking example of this section can be easily generalized for any number and variety of material constitutive models.

The prior plausibility $\pi_{\text{prior}}(M_j|\mathcal{M})$ should be chosen to reflect previous experience about the damage model. Here we picked equal plausibilities of $\frac{1}{2}$ for each damage model.

Figures 8 and 9 show the computed posterior marginal kernel density estimation (KDE) of the parameters for Krajcinovic $\boldsymbol{\theta}_1$ and Marigo $\boldsymbol{\theta}_2$ damage models respectively.

Table 1 shows the computed evidences and posterior plausibility. The computed values indicate that for the given set of reference data, both posterior plausibilities are practically equal to 50%, assuming prior plausibilities of 50%. This means that none of the selected damage models is superior over another in simulating the measured data. This is mainly due to the inadequacy of our information about the system. As indicated previously, both Krajcinovic and Marigo damage models are phenomenological relations postulated based on the uniaxial responses of the material. Therefore using only a set of stress-strain as the set of reference data, not provide enough evidence in order to distinguish between these two damage models. Having more evidence about the evolution of damage in the material (e.g. indirect measurement based upon electrical conductivity fluctuation, complex geometry of the specimen such as 2D and 3D, more complex loading such as localization) could provide more information about the choice of models. It should be noted that the main purpose of such calculation is to prove the feasibility of the developed framework for Bayesian model selection using the notion of model plausibility.

Table 1: Numerical results on log evidence and plausibilities (see (23)). One should note that ρ_{prior} and $\rho_{\text{posterior}}$ are probability mass function (PMF).

Model	Log Evidence $\ln(\pi_{\text{data}}(\mathbf{d}\|M_j))$	Prior Plausibility $\rho_{\text{prior}}(M_j\|\mathcal{M})$	Posterior Plausibility $\rho_{\text{posterior}}(M_j\|\mathbf{d},\mathcal{M})$
M_1:Krajcinovic Damage Model	4024.9	1/2	$\approx 1/2$
M_2:Marigo Damage Model	4025.49	1/2	$\approx 1/2$

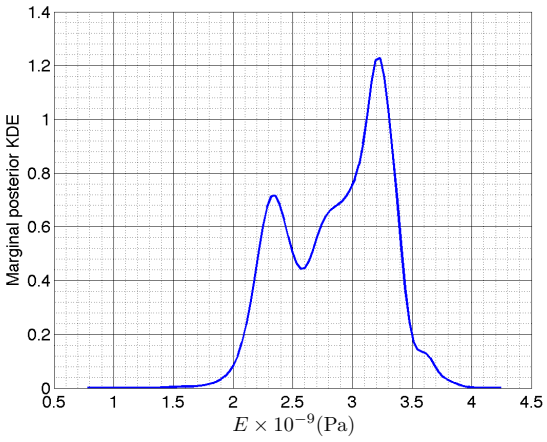

(a)

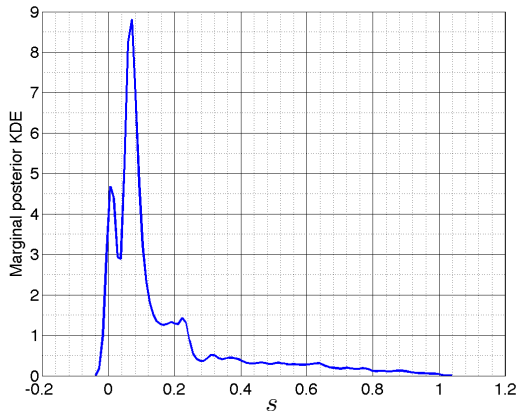

(b)

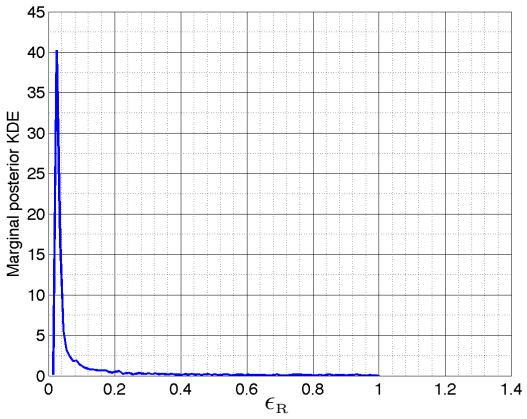

(c)

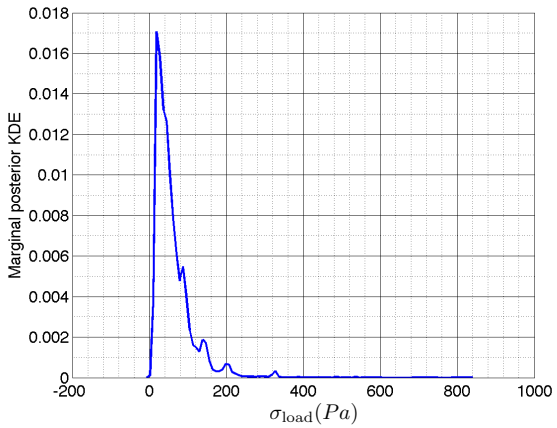

(d)

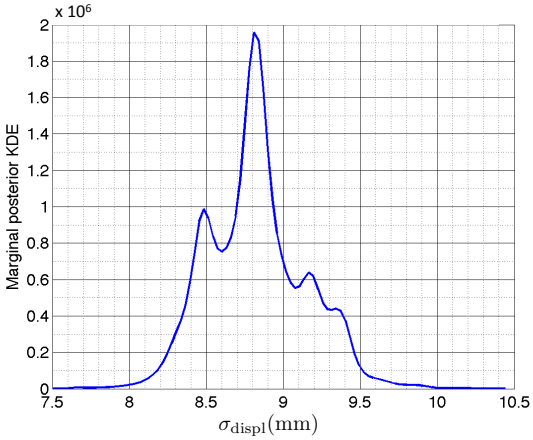

(e)

Figure 8: Calibrated material parameters for Krajcinovic damage model. Posterior marginal density estimation of (a) Elastic modulus; (b) parameter s; (c) parameter ϵ_{R}; (d) σ_{load}; and (e) σ_{disp} [4].

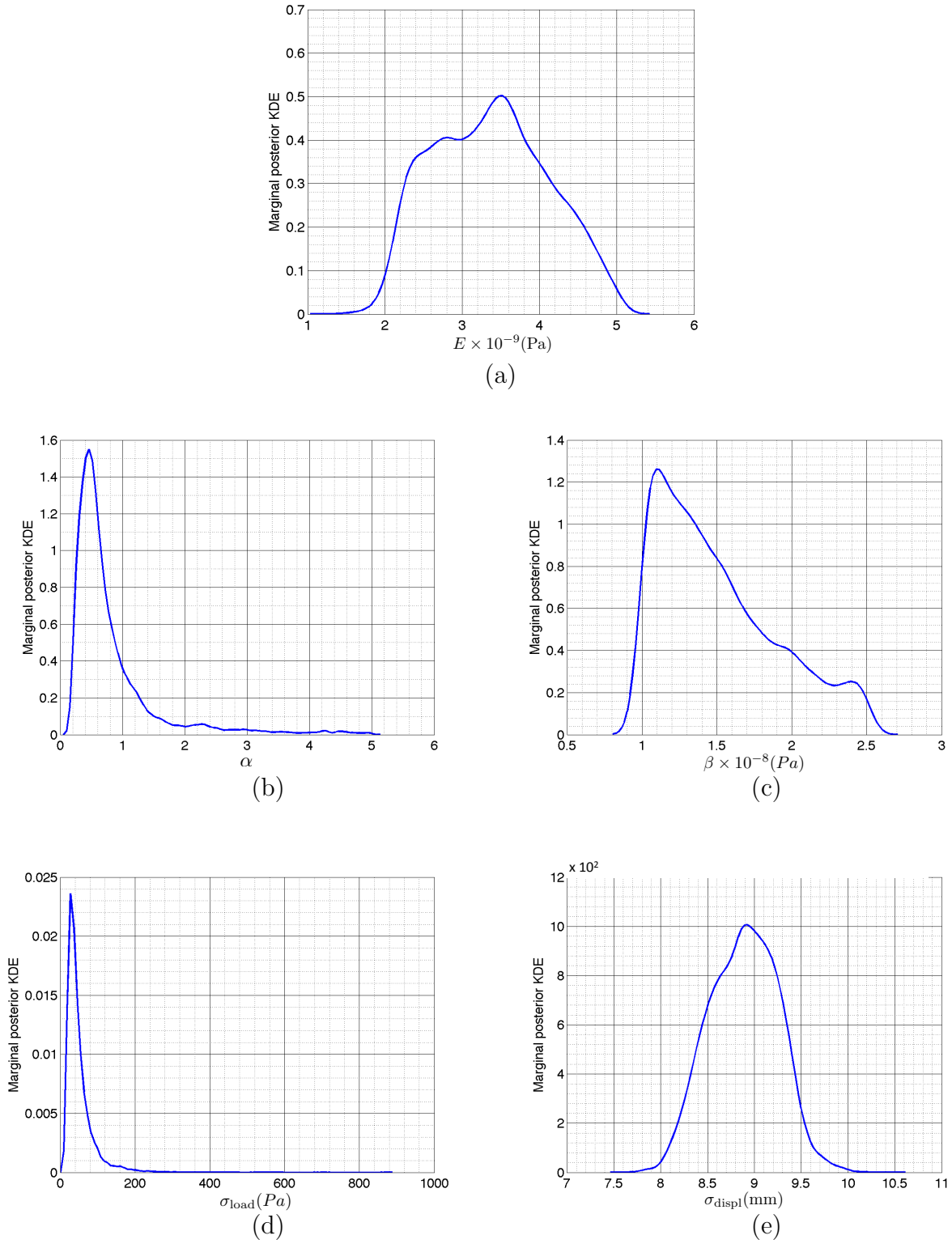

Figure 9: Calibrated material parameters for Marigo damage model. Posterior marginal density estimation of (a) Elastic modulus; (b) parameter α; (c) parameter β; (d) σ_{load}; and (e) σ_{disp}.

7.2 State Monitoring with Extended Kalman Filter

The Extended Kalman Filter is also applied to the damage models listed in Section 2 along with experimental data in order to assess the evolution of the state with time. Before performing the runs for computing the damage growth, we monitor the state of Young's modulus, E, fixing all remaining parameters in M_1, and plot the values of $\hat{\boldsymbol{\theta}}$ from (48). Figure 10 shows the plots. Although the modulus of elasticity is a material property and has a unique value for a particular material, such test helps us to check the stability of the Model Library, judge the correctness of the Top Application code and of the likelihood routines, and gain confidence that the outcome of the implemented Filtering Library make sense. Regardless of the cycles of unloading/reloading, Figure 10 shows the overall loss of stiffness in the material and points to the need to introduce some kind of inelasticity (i.e. damage) into the material model.

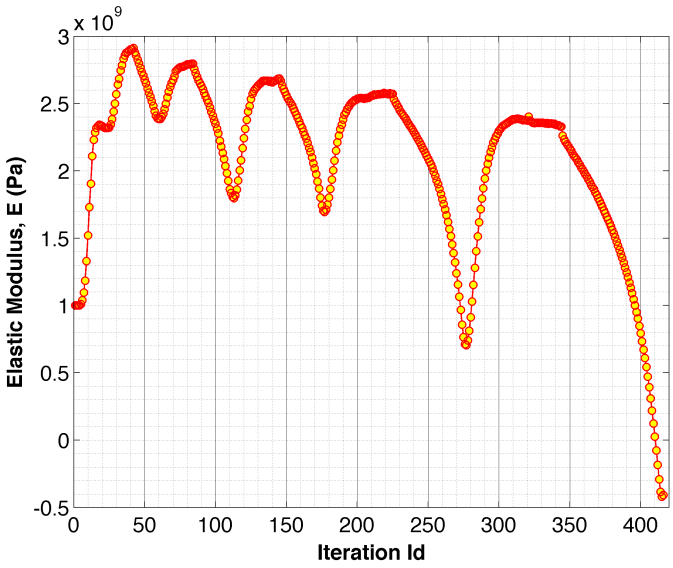

Figure 10: Some check with M_1 to ensure the proper implementation of Extended Kalman Filter. One should note that the variation in Youngs modulus as shown here is *not* represent the reality and this plot mainly is drawn to test the code integration.

Filtering of the evolution of damage predicted by models M_1 and M_2 is performed to statistically evaluate how the damage state develops in the material through time. In this regard, one needs to fix the values of the continuum damage models $(E, \epsilon_{\mathrm{R}}, s)$ in M_1 and (E, α, β) in M_2 with the MAP points of the statistical calibration and filter with only the damage variable, D, throughout the finite element mesh. The fixed deterministic values of model parameters used for the filtering process are shown in Table 2.

The outcomes of the Extended Kalman Filter applied to the Krajcinovic and Marigo damage models, given the experimental data, is shown in Figures 11 to 14. These figures represent the spatial and temporal variation of the damage mean vector and covariance matrix. Figures 11 and 13 shows the damage growth through the time of applied force. As mentioned previously, the deformation due to damage itself can be completely (or partially) recovered upon unloading in which the recoverable part is attributed to micro-cracks closure

upon unloading. Such phenomena is reflected in the so-called *staircase* evolution of the damage variable observed in these figures. Once the load is applied to the specimen, the damage starts to accumulate. Throughout the set of elastic unloading and reloading, the damage variable stays unchanged corresponding to the micro-crack closure. Once the state of straining reaches to the maximum strain experienced by the material up to the present time (i.e. onset of unloading in the current experiment), the damage starts to grow further causing further degradation in the material stiffness. Moreover, these figures indicate that damage variable remains almost constant though the space except the clear jump at the *position id 1.* This is the location of the observed *hot spot* in the experiment as indicated in Figure 2. As mentioned previously, the amount of strain at this location is higher than the average strain in the specimen attributed to the presence of local defect in which the eventual failure of the specimen (i.e. system) occurs. The higher rate of damage growth (material degradation) in this location can be observed in Figures 11 and 13 at the initial stage of the test. Therefore our DDDAS infrastructure enables us to predict the failure in the system given the near real time data, so that we can inform ourselves for potential decisions to be taken about the system, and/or for potential control actions to be taken on it. In addition to the above consideration, the quantitative comparison of the results of using two different continuum damage models used in our numerical experiment indicates that while both models predict the evolution of the material degradation in Krajcinovic model gives higher values of the damage variable at the *position id 1.* As mentioned earlier in this section, we are not able to draw a conclusion regarding which prediction is more accurate due to inadequate information we have about the behavior of the system at this point.

Moreover the overall decrease in the damage covariance matrix shown in Figures 12 and 14 indicates the increase in the level of confidence regarding the damage evolution by having more evidence (i.e. measured data).

Table 2: The fixed deterministic damage model parameters of M_1 and M_2 used for the Extended Kalman filtering.

Model	Model parameters		
M_1: Krajcinovic Damage Model	$E = 1 \times 10^9$(Pa)	$s = 0.06$	$\epsilon_{\mathrm{R}} = 0.08$
M_1: Marigo Damage Model	$E = 1 \times 10^9$(Pa)	$\alpha = 0.95$	$\beta = 1 \times 10^8$(Pa)

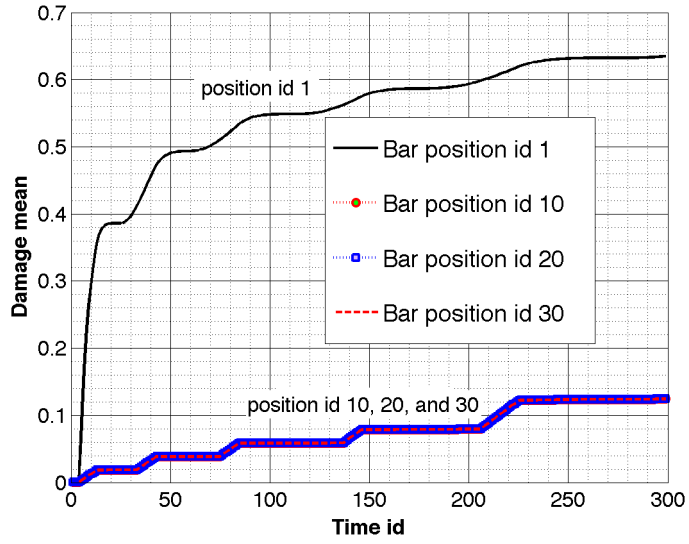

(a)

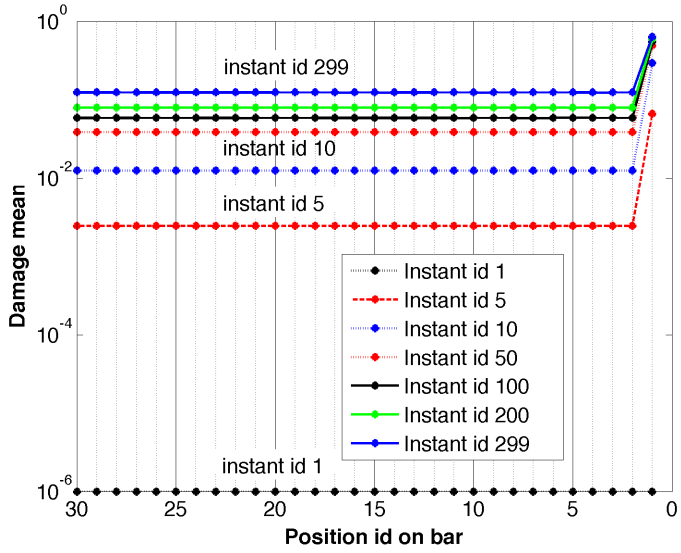

(b)

Figure 11: Evolution of damage mean vector for Krajcinovic damage model with respect to (a) time $t^{(k)}$; (b) position x_i.

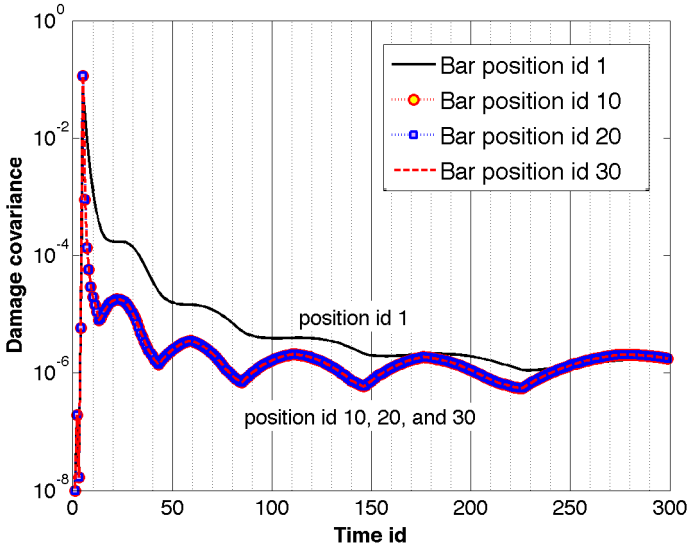

(a)

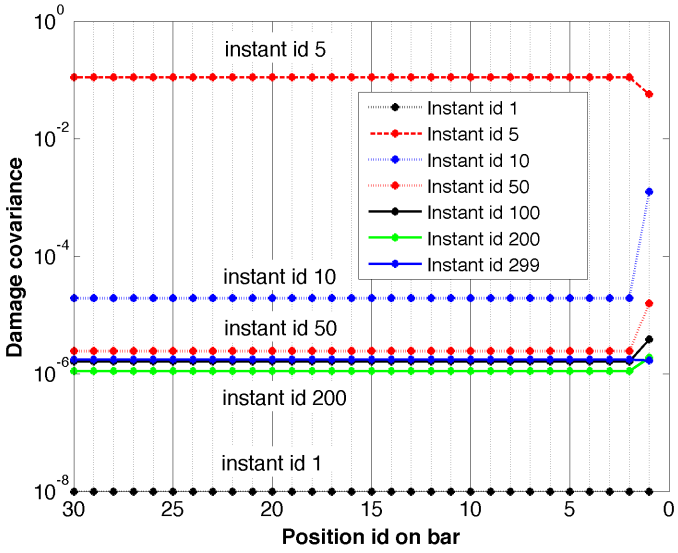

(b)

Figure 12: Evolution of damage covariance matrix for Krajcinovic damage model with respect to (a) time $t^{(k)}$; (b) position x_i.

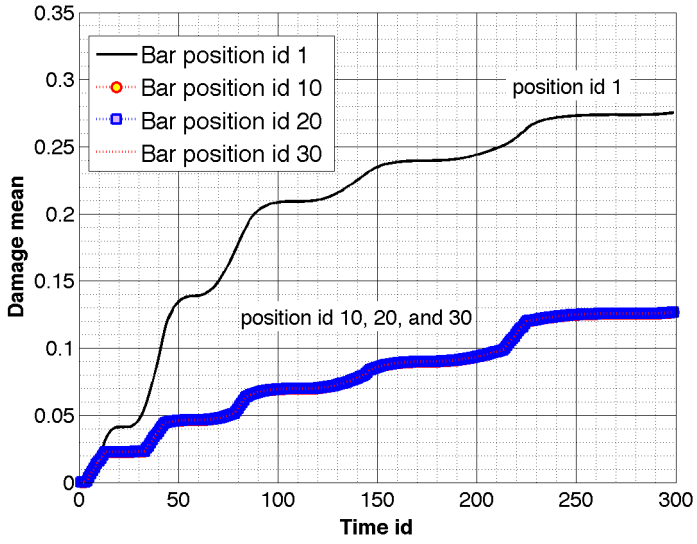

(a)

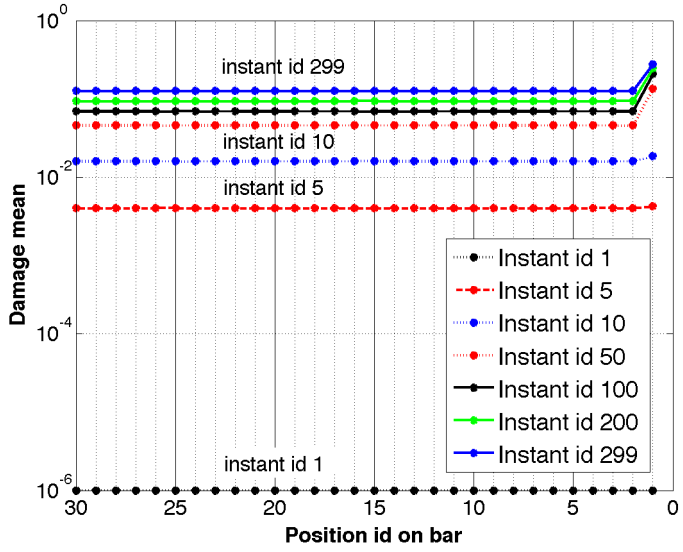

(b)

Figure 13: Evolution of damage mean vector for Marigo damage model with respect to (a) time $t^{(k)}$; (b) position x_i.

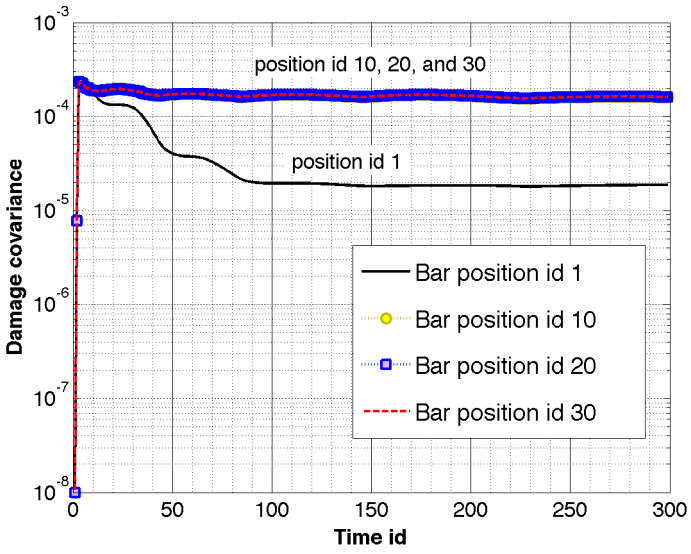

(a)

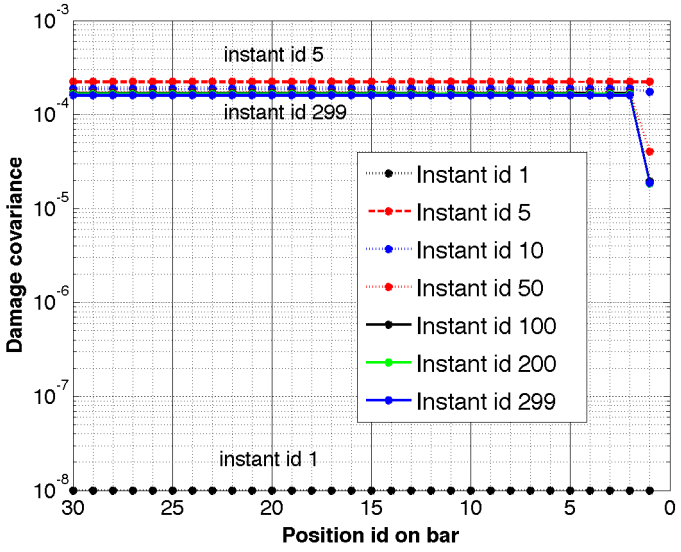

(b)

Figure 14: Evolution of damage covariance matrix for Marigo damage model with respect to (a) time $t^{(k)}$; (b) position x_i.

8 Conclusions

In the present study a new Dynamic Data-Driven Application System (DDDAS) is demonstrated that allows the quantification and measurement of uncertainties in experimental data, model parameters, and in the selection of the model itself for controlling material damage in structural components. Such DDDAS combines the mathematical model of inelastic (i.e. damage) material behavior and the experimental observations with a Bayesian framework for uncertainty quantification, calibration, validation, and model selection. The physical problem under study is the behavior of thin composite structural components such as are common in aircraft structures under loads that can generate distributed damage.

The data of tensile experiments, in term of spatial variation in the strain field and force over time, conducted on carbon nanotube infused epoxy nanocomposites [4] is taken into consideration. Continuum damage theories are used to model the onset and evolution of damage, generally in the form of micro-crack densities. Among the various existing evolution equations for damage that are available in the literature, two damage models Krajcinovic and Marigo are selected for the statistical calibration, model ranking, and real-time monitoring of damage. Moreover, a Bayesian framework for uncertainty quantification, calibration, validation, and selection of models is described in this work. Since the damage growth in the material depends on the underlying dynamics at the micro-scale over time (evolution of micro-crack, micro-voids, etc), Bayesian filtering is applied so that the damage model is calibrated every time additional experimental data is obtained. Particularly the Kalman filter is adopted in this study, enables the damage models to adjust to the new information and update the damage state in real-time.

To implement the DDDAS using the aforementioned constituents, an integrated infrastructure, expressed in software, is developed to incorporate:

1. the numerical algorithms for a finite element solution of the continuum damage models;
2. generated experimental data;
3. algorithms for sampling as well as model calibration, plausibility, and selection based on Bayesian-based methods; and
4. extended Kalman filter procedure;

The outcomes of such integration among experimental evidences, computational damage models, and statistical analyses can be summarized as follow:

- The Bayesian framework used in this study enables statistical calibration of the computational models of physical phenomena (i.e. continuum damage models) against experimental observations, along with quantifying the inherent uncertainties in the data, the model, and the numerical solution approach.
- The developed framework for Bayesian model ranking using the notion of model plausibility is a feasible approach. This has been demonstrated by computing the posterior plausibilities for both Krajcinovic and Marigo damage models given the uniaxial responses of the material.

- Using the Kalman filter for real-time monitoring of the system state evolution with time results in enhancement of predictive models of complex physical phenomena. The computed results show that such approach allows forecasting the location of the concentrated material degradation (leading to system failure) given the data of the initial stage of the test.

Therefore the developed DDDAS infrastructure enables the prediction of failure in the system given the near real time data, allows feedback for potential decisions to be taken about the system, and/or for potential control actions to be taken on it.

In summary, the development of a successful DDDAS infrastructure requires a diverse range of technologies, including precise experimental techniques, micromechanical evolution models of the damage and pre-failure of materials, Bayesian inference, information theory, parallel sampling algorithms, and high performance computing. A demonstration of a system that combines these qualities is given in the present work. The results suggest that the approach described in this study leads to a powerful new technology for developing predictive models of complex physical phenomena in the presence of uncertainties in parameters, data, and the plausibility of computational models for given data histories.

Acknowledgments

The support of this work under AFOSR contract FA9550-11-1-0314 is gratefully acknowledged.

References

[1] Satish Balay, Jed Brown, , Kris Buschelman, Victor Eijkhout, William D. Gropp, Dinesh Kaushik, Matthew G. Knepley, Lois Curfman McInnes, Barry F. Smith, and Hong Zhang. PETSc users manual. Technical Report ANL-95/11 - Revision 3.4, Argonne National Laboratory, 2013.

[2] Satish Balay, Jed Brown, Kris Buschelman, William D. Gropp, Dinesh Kaushik, Matthew G. Knepley, Lois Curfman McInnes, Barry F. Smith, and Hong Zhang. PETSc Web page, 2013. http://www.mcs.anl.gov/petsc.

[3] Satish Balay, William D. Gropp, Lois Curfman McInnes, and Barry F. Smith. Efficient management of parallelism in object oriented numerical software libraries. In E. Arge, A. M. Bruaset, and H. P. Langtangen, editors, *Modern Software Tools in Scientific Computing*, pages 163–202. Birkhäuser Press, 1997.

[4] P. T. Bauman, D. Faghihi, J. T. Oden, E. E. Prudencio, K. Ravi-Chandar, and S. V. Williams. Development of a Stochastic Dynamic Data Driven Applications System for Prediction of Material Damage. AFOSR Report, 2013.

[5] G. Belloni, G. Bernasconi, and G. Piatti. *Creep Damage Models. In: Creep of Engineering Materials and Structures.* Applied Science Publisher, 1979.

[6] J. L. Chaboche. Continuum damage mechanics: Part I - General concepts. *Journal of Applied Mechanics*, 55:59–64, 1988.

[7] J. L. Chaboche. Continuum damage mechanics: Part II - Damage growth, crack initiation and crack growth. *Journal of Applied Mechanics*, 55:65–72, 1988.

[8] S. H. Cheung, T. A. Oliver, E. E. Prudencio, S. Prudhomme, and R. D. Moser. Bayesian uncertainty analysis with applications to turbulence modeling. *Reliability Engineering and System Safety*, 96:1137–1149, 2011.

[9] F. A. Cozzarelli and G. Bernasconi. Non-linear creep damage under one-dimensional variable tensile stress. *International Journal of Nonlinear Mechanics*, 16:27–38, 1981.

[10] F. Darema. DDDAS: Dynamic Data Driven Applications Systems. `http://www.nsf.gov/cise/cns/dddas`.

[11] F. Darema. *Dynamic Data Driven Applications Systems: A New Paradigm for Application Simulations and Measurements*, volume 3038 of *Lecture Notes in Computer Science*. Springer, 2004.

[12] F. Darema. Dynamic data driven applications systems: A new paradigm for application simulations and measurements. In Marian Bubak, Geert Dick van Albada, Peter M. A. Sloot, and Jack J. Dongarra, editors, *Computational Science - ICCS 2004*, volume 3038 of *Lecture Notes in Computer Science*, pages 662–669. Springer Berlin / Heidelberg, 2004.

[13] F. Darema. Grid computing and beyond: The context of dynamic data driven applications systems. *Proceedings of the IEEE*, 93(3):692–697, 2005.

[14] F. Darema. Characterizing dynamic data driven applications systems (dddas) in terms of a computational model. In Gabrielle Allen, Jaroslaw Nabrzyski, Edward Seidel, Geert van Albada, Jack Dongarra, and Peter Sloot, editors, *Computational Science ICCS 2009*, volume 5545 of *Lecture Notes in Computer Science*, pages 447–448. Springer Berlin / Heidelberg, 2009.

[15] F. Darema and M. Rotea. Dynamic data-driven applications systems. In *Proceedings of the 2006 ACM/IEEE conference on Supercomputing*, SC '06, New York, NY, USA, 2006. ACM.

[16] F. Darema and H. E. Seidel. Report of the August 2010 Multi-Agency Workshop on InfoSymbiotic/DDDAS. The Power of Dynamic Data Driven Applications Systems, 2011.

[17] K. C. Estacio-Hiroms and E. E. Prudencio. *Quantification of Uncertainty for Estimation, Simulation, and Optimization (QUESO), User's Manual*. Center for Predictive Engineering and Computational Sciences (PECOS), Institute for Computational and Engineering Sciences (ICES), The University of Texas at Austin, Austin, TX 78712, USA, version 0.45.3 edition, October 2012.

[18] A. M. Fraser. *Hidden Markov Models and Dynamical Systems*. SIAM, 2008.

[19] E. T. Jaynes. *Probability Theory: The Logic of Science*. Cambridge University Press, 2003.

[20] A. H. Jazwinski. *Stochastic Processes and Filtering Theory*. Dover, 1998.

[21] L. M. Kachanov. On time to rupture in creep conditions. *Izviestia Akademii Nauk SSSR*, 8:26–31, 1958.

[22] B. S. Kirk, J. W. Peterson, R. H. Stogner, and G. F. Carey. libMesh: a C++ library for parallel adaptive mesh refinement/coarsening simulations. *Engineering with Computers*, 22(3):237–254, 2006.

[23] D. Krajcinovic and G. U. Fonseka. The continuous damage theory of brittle materials, Parts 1 and 2. *Journal of Applied Mechanics*, 48:809–824, 1981.

[24] C. Lee, F. A. Cozzarelli, and K. Burk. One-dimensional strain dependent creep damage in homogeneous materials. *International Journal of Nonlinear Mechanics*, 21:303–314, 1986.

[25] J. Lemaitre and J. L. Chaboche. *Mechanics of Solid Materials*. Combridge University Press, 1990.

[26] J. J. Marigo. Formulation of a damage law for elastic material. *Count-returned of Acadmie of Sciences. Paris, Srie II*, 292:13091312, 1981.

[27] S. Murakami and N. Ohno. *Continuum theory of creep and creep damage*. Springer, 1981.

[28] J. T. Oden, E. E. Prudencio, and A. Hawkins-Daarud. Selection and assessment of phenomenological models of tumor growth. *Mathematical Models and Methods in Applied Sciences*, 2012, in press.

[29] E. E. Prudencio and S. H. Cheung. Parallel adaptive multilevel sampling algorithms for the Bayesian analysis of mathematical models. *International Journal for Uncertainty Quantification*, 2(3):215–237, 2012.

[30] E. E. Prudencio and K. W. Schulz. The parallel C++ statistical library QUESO: Quantification of Uncertainty for Estimation, Simulation and Optimization. In M. Alexander et al., editor, *Euro-Par 2011 Workshops, Part I*, volume 7155 of *Lecture Notes in Computer Science*, pages 398–407. Springer-Verlag, Berlin Heidelberg, 2012.

[31] Texas Advanced Computing Center TACC. `http://www.tacc.utexas.edu/`, 2008-2012.

[32] G. Welch and G. Bishop. An Introduction to the Kalman Filter. `http://www.cs.unc.edu/~welch/kalman/kalmanIntro.html`, 2006. UNC-Chapel Hill TR 95-041.